IEEE Open Journal of the Communications Society

Received XX Month, XXXX; revised XX Month, XXXX; accepted XX Month, XXXX; Date of publication XX Month, XXXX; date of current version XX Month, XXXX.

Digital Object Identifier 10.1109/OJCOMS.2022.1234567

Directional Antennas for sub-THz and THz MIMO Systems: Bridging the Gap Between Theory and Implementation

DUSCHIA M. BODET AND JOSEP M. JORNET, MEMBER, IEEE

[1]Department of Electrical and Computer Engineering, Northeastern University, Boston, MA 02115 USA

CORRESPONDING AUTHOR: Duschia Bodet (e-mail: bodet.d@northeastern.edu).

This work was supported by the National Science Foundation under Grants CNS-1801857 and CNS-1955004

ABSTRACT Multiple-Input Multiple-Output (MIMO) systems have been proposed to increase the capacity and transmission distance of sub-THz and THz communication systems. Although much work has been done to pave the way for arrays and arrays of subarrays using omnidirectional or semi-omnidirectional antenna elements, few works explore the benefits of directional antenna elements in (sub-)THz MIMO systems. This work presents a brief survey of what has been done for sub-THz and THz multiple antenna systems and builds on the previous work to suggest using more directional antenna elements in sub-THz and THz MIMO systems. The first experimental implementation of a sub-THz diversity scheme is also used to verify the findings. Both the numerical and experimental analyses demonstrate that directional antenna elements in sub-THz and THz MIMO can increase the achievable data rates due to their focusing power and the shape of their radiation pattern.

INDEX TERMS Diversity, Beamforming, Communications, MIMO, sub-THz, THz

I. INTRODUCTION

THE terahertz (THz) and, more specifically, sub-THz band is expected to unlock the high data rates required by future wireless communication systems. Spanning 0.1 to 10 THz, these bands boast bandwidths on the orders of tens of Gigahertz (GHz) that have the potential to enable Terabit-per-second (Tbps) links. Multiple-Input Multiple-Output (MIMO) systems are especially attractive for THz and sub-THz systems. The small wavelength of THz-range frequencies enables very small antenna elements, allowing more antennas to fit in a given area [1]. Furthermore, spatially multiplexed channels will be required to reach the Tbps links desired for THz communications [2], and beamforming can allow systems to overcome the heavy propagation losses experienced by the THz channel with a strong enough signal-to-noise ratio (SNR) to enable high-order modulations. Using the array of subarrays (AoSA) structure that has been presented for large or ultra-massive MIMO (UM-MIMO) systems [3], THz and sub-THz MIMO systems would be able to beamform and spatially multiplex at the same time. In this way, both the benefits of spatial multiplexing and beamforming could be achieved simultaneously.

Thus, theoretically, MIMO and UM-MIMO for sub-THz and THz systems have much potential for the future of wireless communications. However, there is still a substantial gap between these theoretically achievable systems and what has been experimentally shown. As will be discussed further in the related works section, much of the theoretical literature on sub-THz and THz MIMO assumes thousands upon thousands of elements configured in such a way that they dynamically can either perform beamforming or spatial multiplexing [1], [3], [4]. However, the experimental works that have come closest to realizing such a system are phased arrays with less than two hundred elements that either cannot perform spatial multiplexing or cannot be dynamically controlled to both multiplex and beamform simultaneously. Of the works that do transmit separate RF streams, spatial diversity is not fully leveraged [5], [6] or channel knowledge is shared between the transmitter and receiver [7].

Futhermore, most theoretical work discussing THz and sub-THz MIMO assume virtually omnidirectional antenna elements (such as patch antennas). Although these kinds of antenna elements enable the UM-MIMO systems described in [1] and [3], they are difficult to fabricate for high frequen-

This work is licensed under a Creative Commons Attribution 4.0 License. For more information, see https://creativecommons.org/licenses/by/4.0/

cies, and the system required to power and control an array of so many elements can become quite complex. Moreover, directional antennas may be required at the receiving array to ensure that the signals being combined from each antenna are more than just noise. Although some previous works have used directional antenna elements in their experimental platforms [5], [8], [9], there has been no formal analysis of the achievable data rates considering the directionality of antenna elements and the spherical wavefront propagation in line-of-sight (LOS) THz and sub-THz MIMO systems.

In this paper, we argue that a similar performance to the AoSA can be achieved by using a directional antenna element to act as a subarray, and we implement a physical layer implementation to take advantage of diversity in a real (sub-)THz MIMO system using directional antenna elements. We presented preliminary results in [10], [11], and in this paper, we build on our previous work to demonstrate the following contributions:

- THz and sub-THz MIMO channel analysis considering antenna beamwidth and radiation pattern using spherical wavefront propagation
- A physical layer implementation to take advantage of the broadband sub-THz MIMO channel that we test experimentally.
- Experimental results verifying improved performance using directional antenna elements
- Numerical analysis of how the antenna element's directionality affects the capacity, steer-ability, and physical size of THz and sub-THz MIMO systems
- Discussing future challenges and research directions in light of these findings

In Section II, we take a closer look at the related work before describing the system in Section III. We verify our findings in Section IV with numerical analysis and experimental results before offering some further discussion on the trade-offs of using directional antenna elements in Section V. Future directions are given in Section VI and concluding our work in Section VII.

II. RELATED WORK

A. OVERVIEW OF THZ MIMO AND RELATED CHALLENGES

In the past decade, the research on sub-THz and THz MIMO systems has exploded. MIMO and UM-MIMO were suggested for THz systems as a way to overcome the low transmission power and increase link distance through beamforming. UM-MIMO was especially attractive for THz systems given the small wavelength that enables physically small antennas. As a result, many antenna elements can fit in a small area [1]. Since the proposal of UM-MIMO for THz and sub-THz, many challenges have been brought forward [12]–[14]. Chief among these challenges is sub-THz and THz systems' reliance on LOS communications. While traditional MIMO systems at lower frequencies often rely on multi-path channels, sub-THz and THz communications do not have rich scattering to ensure multi-path propagation. Additionally, given the electrically large receiving antenna arrays with respect to the transmission distance of sub-THz and THz LOS MIMO systems, the assumption of planar wavefront propagation no longer holds, and therefore spherical wavefront propagation must be calculated. On top of these challenges, THz and sub-THz systems are meant to be broadband, but channel estimation techniques are often frequency dependent. Thus, the estimations may need to be adjusted for different parts of a broadband spectrum [14].

These nuances complicate the channel model and channel estimation processes for sub-THz and THz MIMO systems [12]. The authors of [15] consider the short-range LOS scenario for sub-THz and THz MIMO systems. The authors explore the antenna separations and link distances that enable optimal performance, but they do not consider the spherical wavefront propagation or the antenna elements' directivity in their analysis.

In light of the heavy processing needed to enable a THz MIMO or UM-MIMO system, there has also been concern about the amount of overhead and complexity of the channel estimation algorithm [12]. The authors of [16] develop a robust mathematical 3D channel model for mobile MIMO THz systems, but their model does not consider directional antenna elements. Meanwhile, the authors of [17] develop a deep convolutional neural network to perform the heavy-duty channel estimation. With the hope of pencil-thin beams from UM-MIMO systems [12], the channel estimation algorithms will need to be robust and able to find the strongest path quickly. Some authors have seen these channel estimation processes as a way to approach joint communications and sensing systems [13], [18] given the flexibility of some UM-MIMO and MIMO systems.

Another challenge for LOS channels is their susceptibility to blockage. Reconfigurable Intelligent Surfaces (RISs) have been proposed as intelligent reflecting surfaces (IRSs) to help combat the blockage issue. In light of this concept, IRS-enabled MIMO has also been explored for THz and sub-THz communications [12], [19], [20], but again these works do not consider MIMO systems with directional antenna elements. The reason for this lack of consideration is likely that the antenna radiation pattern is not often considered to be part of the channel. For lower-frequency communications that use virtually omnidirectional antenna elements, this assumption is acceptable. Even for the single-input single-output (SISO) (sub-)THz scenario with highly directional antenna elements, it is also generally safe to assume the antenna element radiation pattern will not impact the capacity as long as the antenna gain is considered in the link budget, due to the primarily LOS transmissions. For MIMO (sub-)THz systems, however, the radiation pattern of the antenna elements can significantly impact the system performance as we will show in this paper.

B. RELATED WORKS SORTED BY ARRAY ARCHITECTURE

Regarding the antenna array design, three primary array architectures have been presented in literature: the fully connected architecture, the AoSA architecture, and the dynamically connected architecture [4]. Although these are the theoretical goals for THz and sub-THz MIMO systems, very few experimental works fit within these categories. Most follow a phased array architecture. In this section, we describe related works organized by their array architecture.

The **fully connected architecture** allows for full control of each antenna element with a Radio Frequency (RF) chain and a phase shifter. The RF chain enables a distinct data stream to be transmitted along the given antenna, while the phase shifter adjusts the phase of the transmitted or received signal. The authors of [21] present a plasmonic fully connected array architecture for THz communications. In their work, each plasmonic patch antenna is powered by a plasmonic source and modulator. The authors of [22] also suggest a graphene-based array solution in which each array element can be fully controlled. Both these works are theoretical, but to our knowledge, there have been four works that have experimentally demonstrated a fully connected array architecture for sub-THz and THz communications. The authors of [5] use an array of two horn antennas at the transmitter and the receiver to perform polarization multiplexing at 300 GHz. Each transmitter-receiver pair of antennas uses a different polarization to ensure the channels do not interfere with each other. Similarly, the authors of [6] engineer two non-interfering spatial channels at 300 GHz by introducing orbital angular momentum (OAM). The signal coming from each antenna is passed through a spiral phase plate which changes the spatial profile of the beam. Then the two beams are combined to travel together. The process is reversed at the receiver. In [7], the authors use a more traditional spatial multiplexing approach. They design an array of patch antennas operating at 130 GHz with the correct spacing given by [15] to ensure orthogonal channels for spatial multiplexing. In our previous work [**?**], [**?**], we use a fully connected architecture to perform maximal ratio transmission and combining at 130 GHz with horn antennas and to explore some of the practical challenges of sub-THz multiple-antenna systems. In particular, we explored: (1) how back-and-forth reflections between the transmitter and receiver in a short-range LOS system can affect the link performance and (2) how the antenna beamwidth can change the performance as well. The results showed antenna element beamwidth having a noticeable impact on the system performance and led us to characterize the relationship in this work further. It is also worth noting that three of these four experimental sub-THz MIMO implementations use directional antenna elements.

The **array of subarrays architecture** allows for phase-only control of each individual antenna element but full control of each subarray of antennas with an RF chain. First proposed by [3], the AoSA architecture allows for both spatial multiplexing and beamforming, while reducing the system complexity and computational cost by using fewer RF chains than the fully connected architecture. The authors of [23] present an adaptation of the AoSA that introduces overlap between subarrays. In this case not all the antennas that are connected to the same RF chain are adjacent to each other. They see improvements in spectral efficiency, energy efficiency, and hardware complexity. The authors of [24] also build on the AoSA architecture. In their work, they suggest using spatial modulation with each subarray. In this case, only one subarray transmits at a given symbol time, and data is encoded into which subarray is being used. Few works experimentally demonstrate the AoSA architecture. The authors of [25] generate subarrays of eight patch antenna elements at 135 GHz. In [26] a similar array is put forward, in which each subarray can be powered by a separate RF chain, but the authors use the array for digital beamforming instead of spatial multiplexing. Both [26] and [25], are the only experimental works to our knowledge achieving the array of subarrays structure for (sub-)THz systems, and yet their architectures are still a simplified version of the AoSAs approach. The phase difference supplied to each antenna element within a subarray cannot be dynamically controlled by a phase shifter as suggested in [3]. Instead, the phase difference is kept constant and is dictated by a delay line connecting the antenna elements. In this way, each "subarray" could be considered a directional antenna. Because the relative phases between elements are fixed, they will operate as a unit that behaves like a single directional antenna element.

The **dynamically connected architecture** was presented to offer a way to balance the trade-offs of the fully connected and AoSA architectures. In this case, the MIMO system can dynamically adjust how many or how few elements are in each subarray. Essentially, the dynamically connected array can adjust to be fully connected or to be an AoSA using a switching network. Although they have primarily been presented for mm-Wave MIMO systems [27], this work could be extended for THz or sub-THz systems as well. To our knowledge, dynamically connected arrays have yet to be fabricated for sub-THz and THz systems.

In the **phased array architecture**, there is only phase control of the individual antenna elements. In other words, there is only one RF chain connected to the entire array, and therefore only one data stream can be transmitted at a time. For this reason, some might not consider phased arrays to be MIMO systems. Even so, there have been many experimental solutions presenting phased arrays for sub-THz and THz communications. The authors of [28] generate 1 THz beam using a 2x2 element array. The authors of [8] and [9] both demonstrate phased arrays of horn antennas in the 300 GHz range performing beamforming in transmission or reception. The authors of [29] also work in the 300 GHz range to perform digital beamforming in transmission or reception. In

[30] the authors present a 8x16 slot array operating between 130-170 GHz. We would also like to point out that half of these phased arrays (all the works in the 300 GHz range) use horn antennas in the array.

C. THE THZ MIMO GAP

Considering the current body of research around (sub-)THz multiple antenna systems, there is a noticeable gap between what has been envisioned and is considered by theoretical papers and what is currently feasible and practically achievable by experimental works. This gap is two-fold:

1. The lack of a physical layer and channel estimation implementation strategy that can truly leverage a broadband (sub-)THz MIMO system. Of the fabricated experimental platforms that are able to send multiple data streams, none of them fully take advantage of spatial diversity in the (sub-)THz MIMO channel. Of the works that do transmit separate RF streams, data is multiplexed using polarization [5] and/or Orbital Angular Momentum (OAM) [6]. Although polarization and OAM multiplexing are viable ways of creating orthogonal channels, the ability to take advantage of spatial diversity for (sub-)THz MIMO would further improve the capacity of the system. In [7], the authors use a vector network analyzer to collect the channel state information for a spatial multiplexing transmission, but in a practical setting, a communication system should be able to acquire the channel information some other way. There has yet to be a physical layer implementation that takes advantage of spatial diversity over separate RF streams for sub-THz MIMO without any channel knowledge being assumed or shared between the transmitter and receiver. Designing such a physical layer has been an open challenge, and in this paper, we will present a potential implementation along with experimental results verifying its feasibility.

2. The theoretical works only consider systems with omnidirectional antennas while most experimental systems use directional antenna elements. Although the AoSA and the dynamically connected solutions theoretically allow for the dynamic control desired for THz and sub-THz communications, only two such arrays have been fabricated to date. These two arrays, as mentioned earlier, do not even strictly fit into the AoSA category since the phase at each antenna cannot be dynamically controlled by a phase shifter. Furthermore, of all the solutions that have been fabricated, none are close to the UM-MIMO scale (thousands of elements by thousands of elements). This gap between theory and experiments is due to fabrication challenges. Although the research community has all the pieces to build RF chains for MIMO and UM-MIMO systems, keeping a tightly packed set of many of these RF chains together without overheating is an open research challenge that has yet to be solved. Additionally, analog-to-digital converters (ADCs) and digital-to-analog converters (DACs) are physically large and power-hungry devices. Each RF chain would require an ADC/DAC, and therefore a system with more subarrays would need to power and fit these devices close together. Thus beyond fabricating small devices, which is a difficult and costly process [1], the systems that power and control each antenna or subarray also need to be numerous and small but supplied with enough power.

These challenges are still being combated by the research community and likely will be solved one day. In the meantime, however, we propose to achieve a similar performance to the AoSA solution by using directional antenna elements to act as a subarray. In the AoSA architecture, each subarray is a phased array that can beamform to generate an array gain in a certain direction. In other words, each subarray acts as a steerable directional antenna. Thus instead of an array of subarrays, we can achieve similar performance with an array of directional antennas. For antennas to be directional, they must be larger than half the wavelength; the more directional they are, the larger they must be, which makes them much easier to fabricate. Furthermore, instead of requiring power and control for each antenna element within a subarray, it would only be needed for each subarray (ie directional antenna). Furthermore, if using omnidirectional elements at the receiving array, the intercepted power might be so low that it will not breach the noise floor of the ADC. Thus, in some cases, directional antenna elements may be required at the receiving array to ensure that any signal is observed at all.

Although most experimental have used directional antenna elements in their platforms [5], [8], [9], to our knowledge, there has been no formal analysis of the achievable data rates considering the directionality of antenna elements in LOS THz and sub-THz MIMO systems. Thus, we begin this analysis in the next section.

III. SYSTEM MODEL

A. SCENARIO

It is important to consider how a (sub-)THz MIMO system with directional antenna elements will differ from a MIMO system at lower frequencies and/or without directional antenna elements. The diagram shown in Figure 1 helps illustrate these particularities. In general, MIMO systems at lower frequencies rely on multi-path propagation to generate orthogonal channels that can be exploited for spatial multiplexing. However, as listed in the middle oval of Figure 1 sub-THz and THz frequencies suffer higher propagation losses, compared to lower frequency communications which lead to primarily LOS channels. Thus to generate orthogonal channels researchers have proposed using polarization [5], orbital angular momentum (OAM) [6], or optimal antenna spacing to engineer orthogonal channels [7]. Theoretically, these approaches would also work at lower frequencies, but generally, they are not necessary due to the rich scattering environments at traditional radio frequencies. In this paper we focus on the (sub-)THz MIMO LOS channel, given the

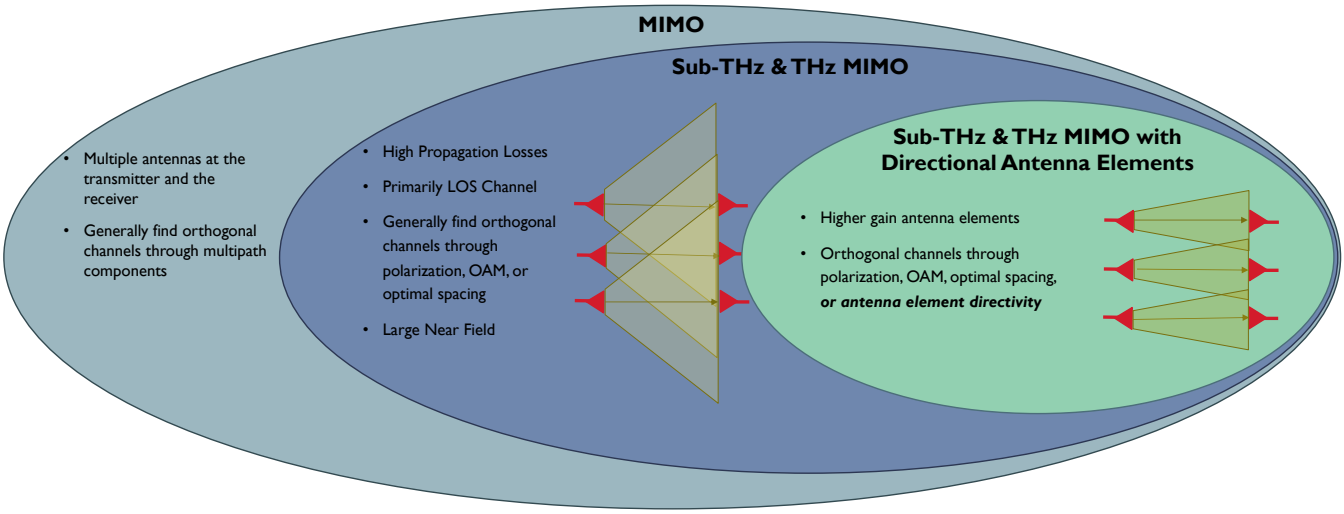

FIGURE 1. **Comparing a (sub-)THz MIMO system using directional antenna elements with MIMO with omnidirectional elements and at lower frequencies**

high path loss and dominance of LOS communications in (sub-)THz regime [14], [15].

In addition to less multipath at (sub-)THz frequencies, The large antenna apertures combined with small wavelengths for (sub-)THz MIMO systems lead to near fields of several to hundreds of meters [31] The near-field boundary is generally given by the Fraunhofer distance: $d_F = D^2/\lambda$, where D is the largest dimension of the antenna and λ is the wavelength given by the speed of light divided by the frequency. Thus, for antenna apertures that are large compared to the wavelength, the far field can start very far indeed. Traditional beamforming methods assume the receiver is in the far field of the transmitter by using the assumption of planar wavefront propagation, but in the near field, this assumption cannot be made. Thus sub-THz and THz MIMO systems will also often operate in near-field environments.

Considering a (sub-)THz MIMO system using directional antenna elements as shown in the smallest oval of Figure 1, each antenna element introduces a gain and there is an additional possibility of generating orthogonal channels through the antenna elements' directivity. This scenario is shown in more detail by Figure. 2, where we assume a LOS channel with negligible multipath. We have an array of directional elements at the transmitter and an array of directional elements at the receiver. In Figure. 2, we show a uniform linear array (ULA), but the same analysis can be easily extrapolated to a uniform planar array (UPA). The transmission distance is given by R, the separation between antenna elements within the array is d_{sep}, and the beamwidth of the directional antenna element is given by $2\theta_{bw}$. To calculate the LOS channel matrix, we will also need to know the distance and angle between the nth transmit antenna and the kth receive antenna.

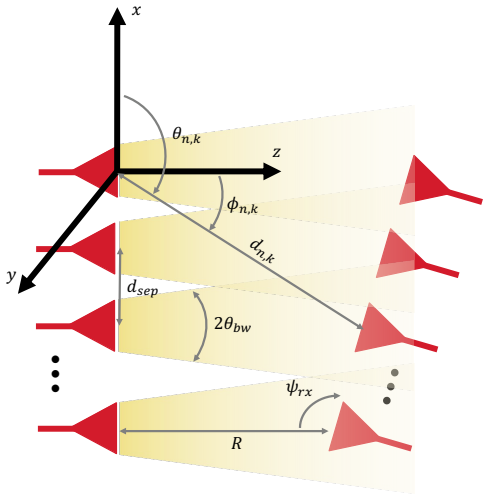

FIGURE 2. **System Model and Parameters**

B. CALCULATING CAPACITY

As presented in [15], the channel matrix will take the form

$$H = \begin{bmatrix} h_{1,1} & \dots & h_{n,1} & \dots & h_{N_{tx},1} \\ h_{1,2} & \dots & h_{n,2} & \dots & h_{N_{tx},1} \\ . & . & & . & . \\ . & . & & . & . \\ . & . & & . & . \\ h_{1,N_{rx}-1} & \dots & h_{n,N_{rx}-1} & \dots & h_{N_{tx},N_{rx}-1} \\ h_{1,N_{rx}} & \dots & h_{n,N_{rx}} & \dots & h_{N_{tx},N_{rx}} \end{bmatrix}, \quad (1)$$

where $h_{n,k}$ is a vector representing the channel between the nth transmit and kth receive antenna. According to [15],

$$h_{n,k} = e^{-j2\pi/\lambda d_{n,k}}, \quad (2)$$

where λ is the carrier frequency wavelength. It is important to remember that this expression depends on the frequency. Another important note is that this expression makes the planar wave propagation assumption that the attenuation

coefficient is very similar between all values of $h_{n,k}$. This assumption holds if the receiver aperture is small enough relative to transmission distance such that all parts of the receiving aperture observe a planar wavefront from the incoming wave. However, this assumption cannot always be made given the short-range applications envisioned for many (sub-)THz communications, combined with the potential for large arrays. Additionally, the radiation pattern of the antenna will cause sub-channels with the same $d_{n,k}$ to observe substantially different gains for various angles. Therefore, spherical wavefront propagation and especially the antenna element's radiation pattern must be considered. Some of the works described in Section II are operating in the near-field of their antenna arrays and where spherical wavefront propagation must be considered [8], [10], [11], [25].

Furthermore, especially for the directional elements we are proposing, the antenna radiation pattern will add an additional consideration in the channel coefficient. In this way, $h_{n,k}$ is given by

$$h_{n,k} = \alpha(d_{n,k}, \lambda)\beta(d_{n,k}, \theta_{n,k}, \phi_{n,k})e^{-j2\pi/\lambda d_{n,k}}, \quad (3)$$

where $\alpha(d_{n,k}, \lambda)$ is the propagation loss which is characterized by the spreading loss and absorption loss: $\alpha(d_{n,k}, f_c) = (\lambda/(4\pi d_{n,k}))\, e^{-K(\lambda)d_{n,k}/2}$, where K is the molecular absorption constant that is a function of frequency [32]. Meanwhile $\beta(d_{n,k}, \theta_{n,k}, \phi_{n,k})$ is the radiation pattern of the antenna and will depend on the antenna element chosen.

Using equation (3) in (1), we can obtain the channel matrix that can be used to calculate the Shannon capacity [33]:

$$C = \log_2 \det \left| \mathbf{I_{N_{rx}}} + \frac{P_{tot}}{N_{tx}} \mathbf{H}\mathbf{H}^{\mathbf{H}} \right| \quad (4)$$

where P_{tot} is the total transmit power, and we assume each transmitting antenna is using the same power.

Another important metric is how many receiving antennas are illuminated by the radiated beam from one transmit antenna. For example, in Figure 2, we have visually shown that the yellow transmitted beam from each transmit antenna is only fully received by one receive antenna. The beamwidth of the directional antenna limits how many transmitted beams reach each receiver. In general, the number of spatial paths per transmit antenna is

$$N_{paths} = \min\left(N_{rx}, N_{illum}\right), \quad (5)$$

where N_{illum} is the number of receiving antennas illuminated by the signal from one transmit antenna. It is given by

$$N_{illum} = \left\lfloor \frac{L_{illum}}{d_{sep}} \right\rfloor, \quad (6)$$

where d_{sep} is the antenna separation shown in Figure 2 and L_{illum} is the length of the receiving array that is illuminated by one transmit antenna. We can use the law of sines to show that

$$L_{illum} = \frac{R \sin\theta_{bw}}{\sin\pi - \psi_{rx} - \theta_{bw}} + \frac{R \sin\theta_{bw}}{\sin\psi_{rx} - \theta_{bw}}. \quad (7)$$

In this analysis, we assume values of ψ_{rx} are close to $\pi/2$ (which would be preferred for arrays with directional antenna elements).

Larger values of N_{paths} generally correspond to higher correlation between spatial channels (i.e., lower rank channel matrices), which can reduce the channel capacity and make spatial multiplexing less feasible [10] As shown in (7), N_{paths} depends upon the transmission distance and the antenna element separation, and beamwidth. In our simulated and experimental results, we proceed to demonstrate further how changing the antenna element beamwidth can significantly impact the system's achievable performance.

IV. ACHIEVABLE PERFORMANCES

A. NUMERICAL ANALYSIS OF CAPACITY INCREASE DUE TO DIRECTIONAL ANTENNA ELEMENTS

The first and perhaps most obvious way directional antenna elements impact the system capacity is through their gain. In Figure 3, we show the capacity as a function of the transmission distance for MIMO systems using dipole, patch, and horn antennas in sub-6G, mm-Wave, sub-THz, and THz bands. For this analysis, we consider half-wavelength dipoles, rectangular patch antennas $\lambda/4$ substrate height, $\lambda/2$ width, and $\lambda/3$ length. Each has a gain of about 8 dBi. The horn antennas are designed according to [34] with their corresponding waveguide dimensions to have the same 20 dBi gain. We assume 100 mW of transmit power that is distributed optimally across sub-bands and sub-channels according to waterfilling. The bandwidth of each system is taken to be 10% of the carrier frequency, and we consider 4x4 arrays of 16 elements at the transmitter and the receiver. We plot the results for dipole antenna arrays in blue, patch antenna arrays in red, and horn antenna arrays in yellow. The line style indicates the frequency. The solid lines are for 2.4 GHz, the dashed lines for 60 GHz, the dotted line for 140 GHz, and the dot-dashed line for 1.05 THz. From Figure 3, we see that as we move to higher frequencies, the increased bandwidth enables higher data rates, especially for shorter distances. As the distance increases, however, the high path loss and noise experienced by the sub-THz and THz channels begin to reduce the achievable performance. We also observe that the horn antenna arrays enable higher capacities than the patch or dipole counterparts. This is primarily due to the gain introduced by the horn antennas.

1) IMPACT OF THE SHAPE OF THE RADIATION PATTERN

This power gain, however, is not the only factor that impacts the MIMO system capacity. The geometry of the LOS system, including the shape of the radiation pattern, can impact the channel matrix, making sub-channels more or less correlated. Taking the 140 GHz scenario as an example, we can see this more clearly in Figure 4 where we have plotted the capacity as a function of the antenna separation. In this case, the transmission distance is kept constant at

This article has been accepted for publication in IEEE Open Journal of the Communications Society. This is the author's version which has not been fully edited and content may change prior to final publication. Citation information: DOI 10.1109/OJCOMS.2023.3318017

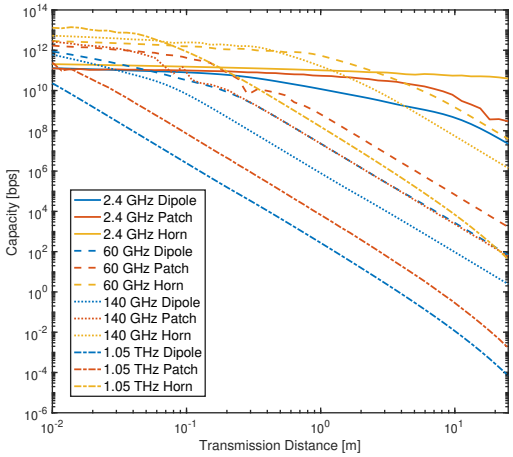

FIGURE 3. Capacity of a MIMO system with 4x4 array at transmitter and receiver

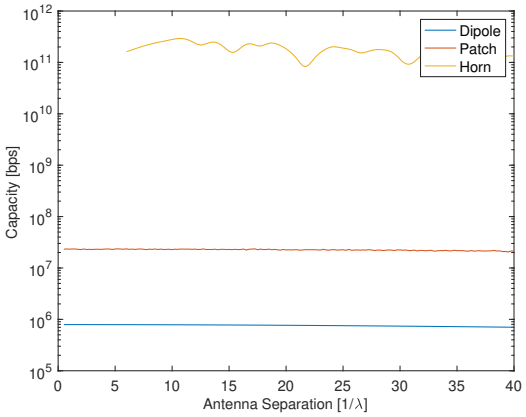

FIGURE 4. Capacity of a 140 GHz MIMO system with 4x4 array at transmitter and receiver

1 m while we sweep the antenna separation. The x-axis is the antenna separation in units of λ, and the y-axis shows the corresponding capacity. Aside from the gain in capacity due to the power gain introduced by the directional elements, the capacity fluctuates as a function of the separation between antennas. These fluctuations are due to the changes in phase and amplitude of each sub-channel as the antenna separation changes. Even though the transmission distance between the transmit and receive arrays remains the same, each $d_{n,k}$ in (2) continues to change leading to changes in phase. Additionally, the azimuth and elevation angles between each transmit and receiving antenna element are also changing which leads to a change in the channel amplitude due to the antenna element's radiation pattern. We can especially see this with the horn antenna array's large variations. The variations are more subtle for the patch and dipole antenna arrays.

To further illustrate that the shape of the radiation pattern alone can impact the capacity, we have used the same

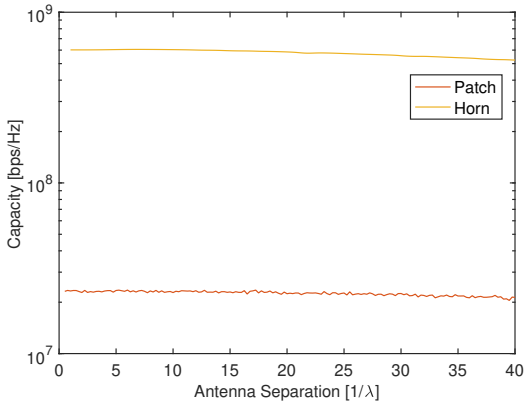

FIGURE 5. Capacity of a 140 GHz MIMO system with 4x4 array at transmitter and receiver with the same gain for the horn and patch antenna

analysis but for a horn antenna designed with an 8 dBi gain (i.e., equal to the dipole gain) in Figure 5. Thus in this scenario, both antenna elements have the same ratio: $\frac{P_{max}}{P_{tot}}$, where P_{max} is the maximum power radiated in a given direction and P_{tot} is the total radiated power. In other words, the maximum power focused along the z-axis is the same for both antennas, but the shape of their radiation patterns differ. Even in this case, the horn antenna array still outperforms the patch antenna array by an order of magnitude. From these results, we can clearly see that directional antenna elements, apart from adding a significant gain without the additional complexity of a phased array, can increase achievable data rates simply by having a less spherical radiation pattern.

2) FREQUENCY DEPENDENCE OF CHANNEL

Another important consideration for THz and sub-THz systems is that they will be broadband systems. Thus, for a given geometrical set-up, the spectral capacity changes for different parts of the spectrum. We can observe these differences in Figure 6, where we plot the spectral capacity for the 140 GHz and 1.05 THz 16x16 MIMO system. The spectral capacity is shown in the color scale while we have frequency on the x-axis and antenna separation on the y-axis. For the case with horn antenna elements, we can see as we did in Figure 3 that the overall capacity is higher. We can also see that the capacity tends to decrease as the frequency increases in addition to an absorption line at 1.1 THz. Thus for broadband systems, some frequencies would see a better channel than others.

We also note that the horn antenna arrays would likely be physically larger than arrays of patches. In Figure 6c and f, the capacity is set to zero for antenna spacings that are not feasible (i.e., smaller than the dimensions of the horn antenna). Analysis of the trade-off between the size of the array will be further explored in Section V, but from this analysis, we have shown that the shape of an antenna

This article has been accepted for publication in IEEE Open Journal of the Communications Society. This is the author's version which has not been fully edited and content may change prior to final publication. Citation information: DOI 10.1109/OJCOMS.2023.3318017

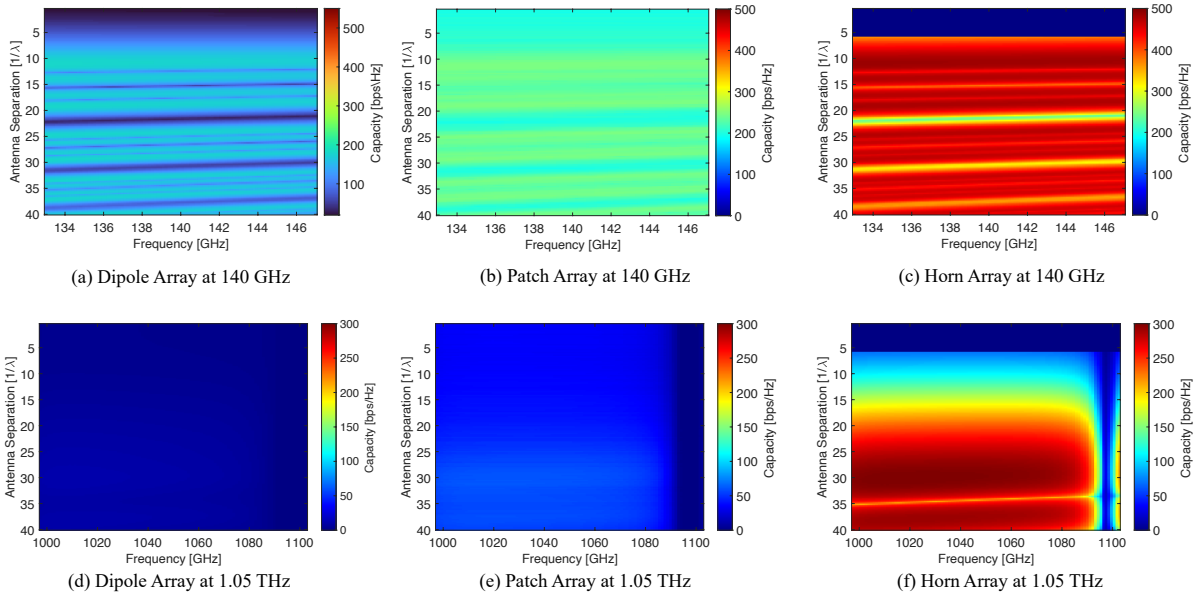

(a) Dipole Array at 140 GHz (b) Patch Array at 140 GHz (c) Horn Array at 140 GHz

(d) Dipole Array at 1.05 THz (e) Patch Array at 1.05 THz (f) Horn Array at 1.05 THz

FIGURE 6. Capacity as a function of distance and frequency

element's radiation pattern can provide an improvement in performance.

B. EXPERIMENTAL RESULTS FROM SUB-THZ MIMO SYSTEM

We were able to verify these findings with experimental results. We leverage the TeraNova test bed as a 2x2 fully connected MIMO architecture, operating at a center frequency of 137.5 GHz with 10 GHz of bandwidth. The testbed is shown in Figure 7 with the system block diagram. The waveform should be equalized in the frequency domain because the channel will be frequency-selective even without any multipath. We observed this frequency dependence of the channel in Figure 6. In addition, the hardware components will also impart a frequency-dependent response on the waveform. Thus, a waveform that can be easily equalized in the frequency domain is preferable. The most likely choice for such a system is an OFDM waveform. However, OFDM signals have high peak-to-average power ratios (PAPRs). Signals with high PAPRs must be radiated with a lower average power so as not to damage the hardware or clip the signal. Because (sub-)THz systems already struggle with low transmit power and will be combatting more noise over their broad bandwidths, signals with low PAPR are favored. For these reasons we use DFT-s-OFDM to facilitate easier frequency-domain equalization while keeping a low peak-to-average power ratio (PAPR) [35]. To leverage the spatial diversity of the system we implement the Alamouti scheme [36]. The parameters for the experimental setup are shown in Table 2. We chose the 1 m transmission distance for practical in-lab testing, but since our set-up does not require a wired connection between the transmitter and the receiver, we could easily increase the transmit distance, especially if we used higher gain antennas. (For reference, the TeraNova test bed has supported sub-THz links from tens of meters [37], [38] to 2 km [39].) The two transmitted waveforms are generated in MATLAB at an intermediate frequency (IF) of 7.5 GHz, before they are passed to a high-speed digital-to-analog converter (DAC). The DAC then sends the analog IF signals to two separate upconverter front-ends that bring the signal to the transmission frequency of 140 GHz. The front-ends are also supplied with a local oscillator (LO) signal of 32.5 GHz that encounters two frequency doublers before it is mixed with the IF signal. On the receiver side, the downconverting front-ends bring the signal back to its IF using an LO. The IF signals are digitized and stored for processing and demodulation in MATLAB. More details on the TeraNova testbed hardware and how the hardware can be configured as a sub-THz MIMO system are in our previous works [10], [11], [40].

For this physical layer, data bits were organized into a frame. The first portion of the frame consisted of an 18-bit Maximum Length Sequence modulated as a BPSK for time synchronization. Both transmitters use the same time synchronization sequence. This sequence is followed by a pilot sequence, which is a random string of bits - unique to each transmitter - that are modulated using the DFT-s-OFDM Alamouti scheme. After the pilot sequence, the data portion of the frame follows. For our experiments, we used 4 DFT-s-OFDM symbols for the pilot and 32 DFT-s-OFDM symbols in the data portion of the frame. We also used a 10% cyclic prefix to eliminate inter-symbol interference. At the receiver, after removing the cyclic prefix and demodulating the DFT-s-OFDM symbols to baseband, we perform channel estimation using a scaled least squares (SLS) algorithm [41] on the received pilot symbols. We use $\gamma_0 = \frac{1}{tr(R_H)}$ as our

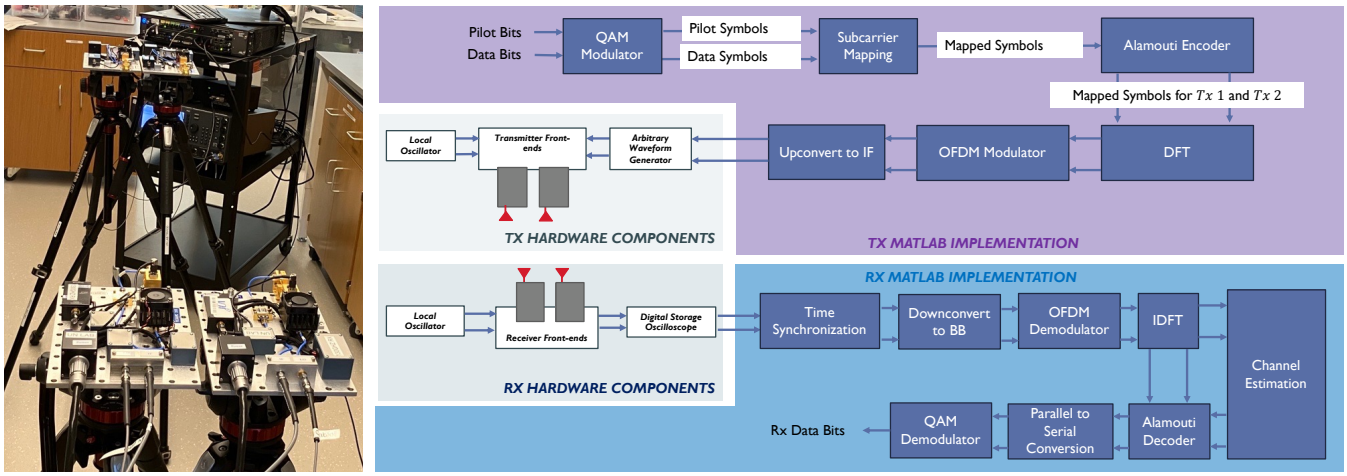

FIGURE 7. **Experimental Set-up and Block Diagram**

scaling factor for the (SLS) estimate, where $R_H = H_{LS}^H H_{LS}$ is the correlation matrix of the least squares (LS) estimate, and $tr\,(.)$ indicates the trace of a matrix.

TABLE 1. **Experimental results for SISO versus the proposed MIMO physical layer showing Error Vector Magnitude (EVM) and Bit Error Rate (BER)**

Scenario	Data Rate	BER
SISO Single-Carrier	32.3 Gbps	$3.89 * 10^{-2}$
SISO DFT-s-OFDM	32.6 Gbps	$4.04 * 10^{-2}$
MIMO PHY Layer (Proposed)	32.1 Gbps	$3.26 * 10^{-4}$

1) OUR MIMO PHYSICAL LAYER VS COMPARABLE SISO SYSTEMS

We start by comparing the performance of our MIMO physical layer to the comparable SISO system. In this analysis we send three waveforms: First, a SISO single-carrier waveform modulated with 512-QAM to reach 32.3 Gbps; second, a SISO DFT-s-OFDM waveform modulated with 256 subcarriers using 16-QAM to reach 32.6 Gbps; and third, the MIMO DFT-s-OFDM Alamouti waveform also modulated with 256 subcarriers using 16-QAM to reach 32.1 Gbps. The SISO and MIMO implementations of DFT-s-OFDM have slightly different data rates because the frame structure is marginally adjusted to be better suited for the MIMO case. The SISO DFT-s-OFDM waveform performs channel estimation as part of the OFDM demodulation step using a subset of the subcarriers. Meanwhile, our MIMO implementation concentrates the pilot symbols at the beginning of the frame. However, the same percentage of the frame is used for pilot symbols whether the pilot is separated from the data portion of the frame in time or in frequency. The resulting bit error rates (BERs), are shown in Table 1, and we can see that the MIMO implementation outperforms both SISO cases by two orders of magnitude. The received constellations are shown in Figure 8 with the blue dots indicating correctly demodulated symbols, red dots indicating incorrectly demodulated symbols, and * marking the transmitted symbols. It is clear that the MIMO case outperforms the SISO scenarios, and thus that our implementation provides a viable approach to leveraging spatial diversity for sub-THz MIMO systems.

2) EVALUATING THE IMPACT OF ANTENNA ELEMENT RADIATION PATTERN

To compare the performance of the system with elements of different directivities, we start by using 21 dBi horn antennas with a half-power beamwidth of 12 degrees for all the transmitting and receiving front ends and compare with the performance when we use 15 dBi antennas with a half-power beamwidth of 33 degrees at the transmitters instead. In each scenario, we transmit the same waveform and implement the same channel estimation and demodulation process in MATLAB. The results are displayed in Table 3. In the full power cases, we transmit with the maximum available transmit power. To investigate the sole impact of the shape of the antenna elements' radiation patterns and not 6 dB power gain introduced by the 21 dBi antennas, we also recorded the results when we reduce the transmit power to see the same received power at each receiving antenna. From Table 3, we see that the more directional antennas provide a substantially lower Error Vector Magnitude (EVM) and Bit Error Rate (BER) in both scenarios. Thus, as shown in our numerical analysis, we can also experimentally see that using directional antenna elements can greatly improve the performance of sub-THz MIMO systems due both to the power gain introduced by the antenna elements as well as the shape of their radiation pattern.

V. TRADE OFFS

Thus, directional antenna elements can increase the achievable capacities, however, they also come with their own set of trade-offs, namely reduced steer-ability and potentially

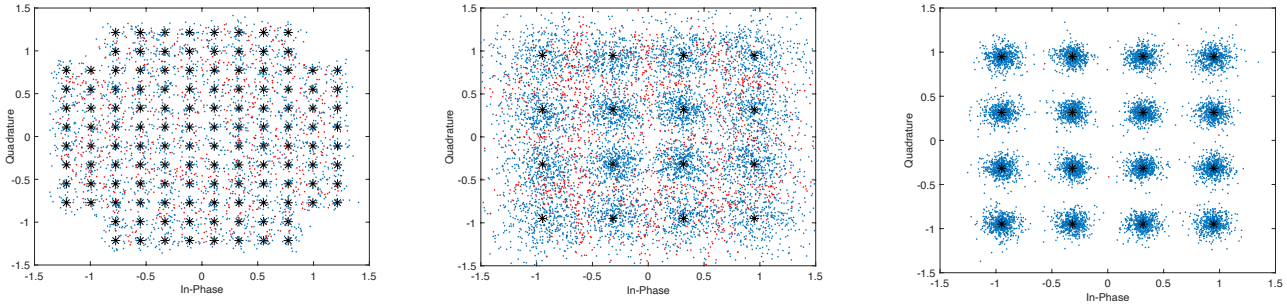

(a) SISO Single-Carrier (b) SISO DFT-s-OFDM (c) MIMO DFT-s-OFDM Alamouti

FIGURE 8. **Received Constellations for Experimental SISO versus MIMO Physical Layer**

TABLE 2. **Parameters for experimental results**

Transmission Distance	1 m
Antenna Separation	17 cm
Data Rate	32.1 Gbps
Bandwidth	10 GHz
Modulation	16 QAM (DFT-s-OFDM)
Number of Subcarriers	256
DFT Spread Length	32

TABLE 3. **Experimental results showing Error Vector Magnitude (EVM) and Bit Error Rate (BER)**

Scenario	EVM	BER
21 dBi Antennas — Full Power	10.7%	$3.93 * 10^{-4}$
21 dBi Antennas — Reduced Power	22.0%	$2.08 * 10^{-2}$
15 dBi Antennas — Full Power	30.3%	$5.55 * 10^{-2}$

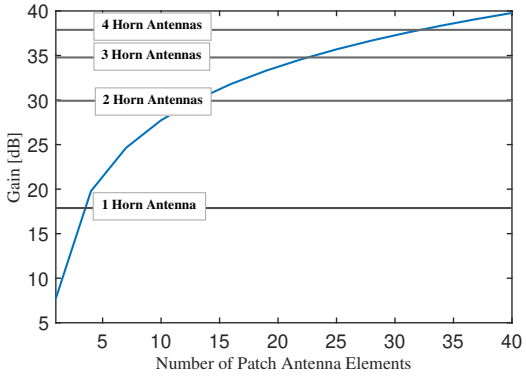

FIGURE 9. **Number of patch antenna elements required for a given gain**

physically larger antenna arrays. We proceed to explore those trade-offs in this section.

One potential challenge to using directional antenna elements in an array as opposed to more omnidirectional elements such as dipole or patch antennas, is the fact that highly directional elements reduce the array's ability to steer. In the case where a sub-array is being replaced with a directional element, in order to dynamically steer the element, an electronically steerable, directional antenna should be used. More research should be done to explore options for this case. One option is the leaky-wave antenna [42] which we discuss further in Section VI.

Another potential option is to use a smaller sub-array of directional antennas. In this case, we will likely still see reduced steer-ability with respect to the sub-array of omnidirectional or semi-omnidirectional elements. For the horn antenna, we take the specifications given in [9] of the horn antennas used in a 4-element ULA. For the patch antenna we use a height of $150\mu m$, with $\epsilon_r = 3.5$, and the width given by [34] $W = \lambda\sqrt{2/(\epsilon_r + 1)}/2$. Both elements are designed to operate at 300 GHz.

The first observation we can make is perhaps an obvious one: when replacing a horn antenna with an array of omni-directional or semi-omnidirectional antennas it will require more of the smaller elements to achieve the same gain as the horn. Comparing the patches and horns described above, for example, each horn antenna achieves a 17 dBi gain, while each patch observes a 7.7 dBi gain. It would take about 3 of these patch antennas working together to produce the gain produced by a single horn antenna.

As shown in Figure 9, the number of patch antennas required to generate the equivalent gain of an array of horn antennas grows rapidly. Although the patch antenna elements are smaller than the horn elements, it will still take physically larger array dimensions to use this array of patches to generate a gain similar to that of the array of horns. In this case, with the dimensions provided above it can be found that for a ULA, the largest dimension of a 4-element patch array (that would be equivalent to one horn element) would be 19 mm, which is larger than the 3mm largest dimension of the horn antenna.

So directional elements certainly provide the most gain in a given direction, but less directional elements are generally more easily steered when they are put into an array.

The steering capabilities of a 4-element uniform linear horn and patch antenna array operating at 300 GHz are shown in Figure 10. We assume a bandwidth of 40 GHz. The radiation pattern at the center frequency is shown in

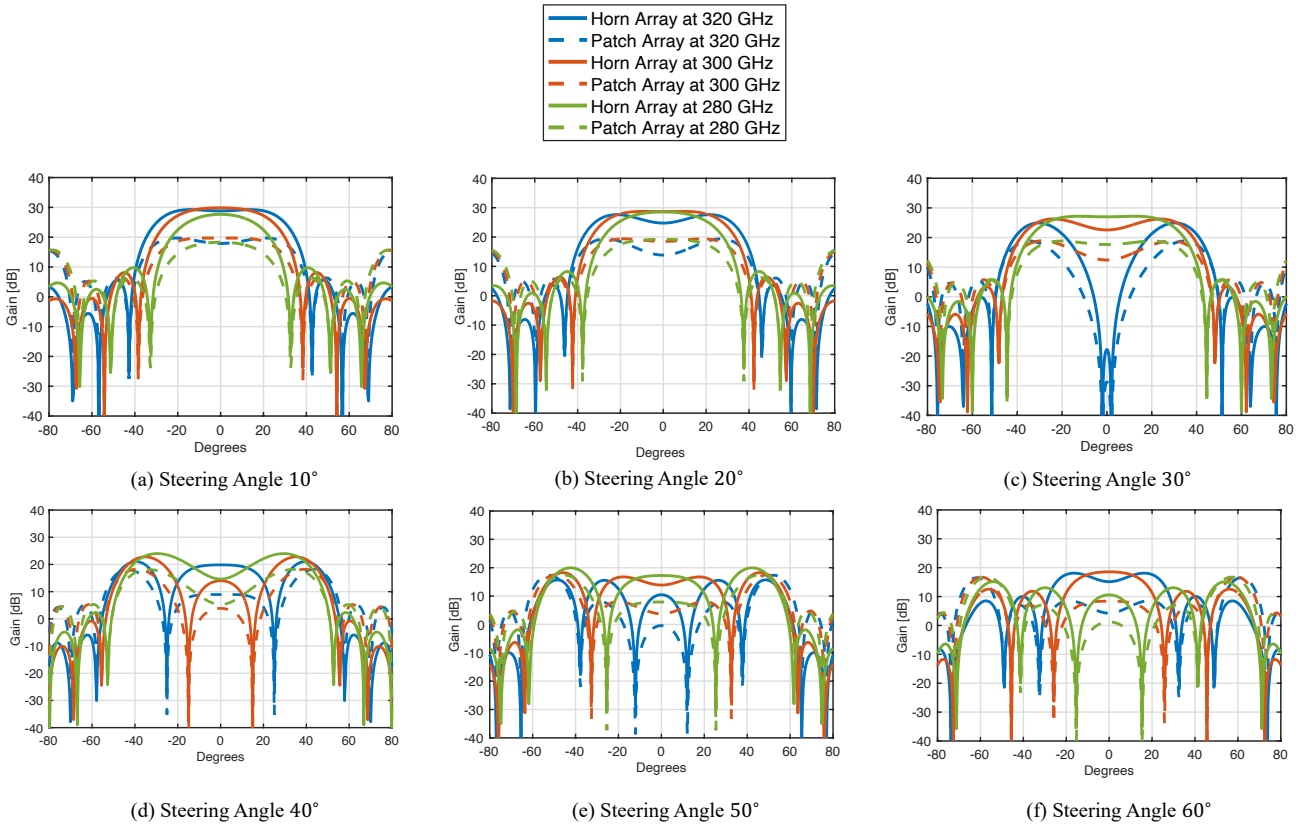

(a) Steering Angle 10° (b) Steering Angle 20° (c) Steering Angle 30°

(d) Steering Angle 40° (e) Steering Angle 50° (f) Steering Angle 60°

FIGURE 10. Steering Capabilities of 4-element Horn and Patch Antenna Arrays

red, while the pattern at the lower and upper bounds of the spectrum are shown in green and blue, respectively. The horn array's radiation pattern is represented by the solid lines, while the patch array's is represented with dashed lines. Even though the half-power beamwidth of the horn array is 40 degrees while the half-power beamwidth of the patch array is 120 degrees, from Figure 10, we can see that the horn array still outperforms in terms of the amount of gain in the desired direction up to about 50 degrees either side (100 degrees total).

Thus opting for an array of horns instead of an array of patches could provide sufficient steer-ability for many applications. Furthermore, it is important to consider the broadband impact when steering such an antenna. Assuming a 40 GHz bandwidth, the blue and green lines show the lower and upper bounds of the spectrum. For both the patch and horn antenna arrays we see the beamsquint effect. In other words, the edges of the spectrum are radiated in a slightly different direction from the center frequency beam. The beamsquint for the patch and horn arrays is comparable.

VI. FUTURE DIRECTIONS AND CHALLENGES

Thus, arrays of directional antenna elements provide a substantial gain in capacity as shown in Section IV, are feasible to build (both from a complexity standpoint as well as considering practical size constraints) and can provide adequate steering capabilities for some scenarios, with comparable broadband performance to more traditional patch antenna arrays. We have shown that they have the potential to bridge the gap between the theoretical and experimental (sub-)THz MIMO works. From here, we discuss some future research directions and challenges continuing to consider directional antennas in MIMO (sub-)THz systems.

A. DETERMINING THE OPTIMAL ANTENNA ELEMENT

There are many options when it comes to directional antennas that could be used in THz and sub-THz MIMO systems. Horn antennas have been widely used in experiments and theory. They can provide significant gain, but can only be steered mechanically. Recently graphene-based antennas have been put forward for some (sub-)THz MIMO solutions [21], [22]. These can be steered dynamically, but currently the power for such devices is extremely low. One option that could offer high power and dynamic steering is the leaky wave antenna (LWA) that has been proposed for mm-Wave, sub-THz, and THz communications. Usually, LWAs can be steered dynamically by changing their operating frequency [43], but the authors of [42] present an architecture that can dynamically steer at a given frequency. The usable bandwidth for a LWA, however, can still be limited.

The horn, graphene-based, and leaky wave antennas are just three options that we have seen put forward in research as a directional antenna element. More work should explore what the ideal antenna element is for sub-THz and THz systems and specifically for MIMO.

B. ENGINEERING NON-INTERFERING CHANNELS

The achievable rates given in our capacity analysis from Section IV assume the transmitter and receiver have perfect channel knowledge. This knowledge enables the transmitter to send the data streams on paths that the receiver is able to differentiate. When the channels are too similar, differentiation is impossible. In the LOS scenario, we can achieve differentiation by engineering the geometry of the system such that the path lengths between each transmitting and receiving antenna introduce a significant phase difference [7]. We could also create non-interfering channels by using a very tight antenna element beamwidth such that each receiving antenna only observes the signal from one transmitting antenna. Future work should explore what other methods can be used to engineer non-interfering channels. Distributed MIMO has been explored at lower frequencies [44], but we have yet to see this work extrapolated to the sub-THz and THz range. As mentioned in Section II, orbital angular momentum (OAM) [6] and polarization multiplexing [5] have been used to engineer non-overlapping channels. In the future, these methods could be explored further along with other ways to engineer orthogonality between data streams.

C. DESIGNING FOR BROADBAND SYSTEMS

The analysis presented in Section IV of this paper is a function of frequency, and in Figure 6, we demonstrate that the capacity of a given scenario varies with frequency. Therefore, designing broadband systems can be particularly challenging because one part of the spectrum may have a better channel than another part of the spectrum. When considering multiple-antenna systems for beamforming, this phenomenon results in the beamsquint effect where different frequencies within the same signal spectrum are pointed in slightly different directions. True time delay (TTD) lines are one way to combat this challenge from a hardware perspective [12], but they make systems less reconfigurable. When considering multiple-antenna systems for spatial multiplexing, this frequency dependence can result in certain parts of the spectrum being able to support spatial multiplexing while other parts of the spectrum cannot support it or cannot support it very well. One possible solution to this challenge is using a multi-carrier modulation scheme and performing the pre-coding step (whether for beamforming or for spatial multiplexing) digitally for each subcarrier. Multi-carrier schemes, however, are poorly suited to THz communications due to their high peak-to-average-power ratios (PAPRs). In this work, we used DFT-s-OFDM to address this challenge, but there could be other approaches, such as using frequency domain equalization with a single-carrier MIMO system. Thus exploring broadband waveform design for THz MIMO systems is an important open research challenge.

D. COMMUNICATING IN THE NEAR FIELD

So far the research community has often assumed to be operating in the far field of the antenna array. Although considering spherical wavefront propagation is a good first step to characterizing behavior in the near field, it is important to remember that true beamforming is not possible in the near field. Instead, we can do beamfocusing or look into other near-field solutions [21]. Even if we move away from traditional beamforming, using larger antenna elements leads to a larger near field, and future work should more fully characterize what that might look like and how it might be leveraged for high-speed communications.

E. LEVERAGING MACHINE LEARNING

There have been many works in literature advocating for deep learning techniques to aid in channel estimation for (sub-)THz MIMO systems [17], [18], [45], [46]. Especially considering the LoS scenario of most (sub-)THz systems combined with likely near-field communications, systems will be required to perform with high accuracy under conditions that could change rapidly. Considering how these approaches might change with directional elements as well as what kind of data sets are necessary to be collected in order to enable properly trained systems are important questions that could inform future theoretical and experimental works.

VII. CONCLUSION

In this paper, we have proposed using directional antennas instead of subarrays in sub-THz and THz MIMO systems. We have shown that directional antennas can improve the achievable data rates of LOS MIIMO systems. Experimentally, we have provided the first implementation of a sub-THz diversity system to verify our findings. We went on to describe some future challenges and research directions that should be explored in light of our findings. We hope this work encourages more cohesion between future theoretical and experimental (sub-)THz MIMO research.

ACKNOWLEDGMENT

This work was supported by the National Science Foundation under Grants CNS-1801857 and CNS-1955004.

REFERENCES

[1] I. F. Akyildiz and J. M. Jornet, "Realizing ultra-massive mimo (1024× 1024) communication in the (0.06–10) terahertz band," *Nano Communication Networks*, vol. 8, pp. 46–54, 2016.

[2] M. Polese, X. Cantos-Roman, A. Singh, M. J. Marcus, T. J. Maccarone, T. Melodia, and J. M. Jornet, "Coexistence and spectrum sharing above 100 ghz," *Proceedings of the IEEE*, 2023.

[3] C. Lin and G. Y. L. Li, "Terahertz communications: An array-of-subarrays solution," *IEEE Communications Magazine*, vol. 54, no. 12, pp. 124–131, 2016.

[4] B. Ning, Z. Tian, Z. Chen, C. Han, J. Yuan, and S. Li, "Prospective beamforming technologies for ultra-massive mimo in terahertz communications: A tutorial," *arXiv preprint arXiv:2107.03032*, 2021.

[5] C. Castro, R. Elschner, T. Merkle, and C. Schubert, "100 gbit/s terahertz-wireless real-time transmission using a broadband digital-coherent modem," in *2019 IEEE 2nd 5G World Forum (5GWF)*. IEEE, 2019, pp. 399–402.

[6] H. Zhou, X. Su, A. Minoofar, R. Zhang, K. Zou, H. Song, K. Pang, H. Song, N. Hu, Z. Zhao *et al.*, "Utilizing multiplexing of structured thz beams carrying orbital-angular-momentum for high-capacity communications," *Optics Express*, vol. 30, no. 14, pp. 25 418–25 432, 2022.

[7] M. Sawaby, B. Grave, C. Jany, C. Chen, S. Kananian, P. Calascibetta, F. Gianesello, and A. Arbabian, "A fully integrated 32 gbps 2x2 los mimo wireless link with uwb analog processing for point-to-point backhaul applications," in *2020 IEEE Radio Frequency Integrated Circuits Symposium (RFIC)*. IEEE, 2020, pp. 107–110.

[8] T. Merkle, A. Tessmann, M. Kuri, S. Wagner, A. Leuther, S. Rey, M. Zink, H.-P. Stulz, M. Riessle, I. Kallfass *et al.*, "Testbed for phased array communications from 275 to 325 ghz," in *2017 IEEE Compound Semiconductor Integrated Circuit Symposium (CSICS)*. IEEE, 2017, pp. 1–4.

[9] S. Rey, D. Ulm, T. Kleine-Ostmann, and T. Kiirner, "Performance evaluation of a first phased array operating at 300 ghz with horn elements," in *2017 11th European Conference on Antennas and Propagation (EUCAP)*. IEEE, 2017, pp. 1629–1633.

[10] D. M. Bodet and J. M. Jornet, "Impact of antenna element directivity and reflection-interference on line-of-sight multiple input multiple output terahertz systems," in *2022 3rd URSI Atlantic and Asia Pacific Radio Science Meeting (AT-AP-RASC)*. IEEE, 2022, pp. 1–4.

[11] J. Hall, D. Bodet, and J. M. Jornet, "Experimental demonstration of multiple input multiple output communications above 100 ghz," in *IEEE INFOCOM 2022-IEEE Conference on Computer Communications Workshops (INFOCOM WKSHPS)*. IEEE, 2022, pp. 1–2.

[12] C. Han, L. Yan, and J. Yuan, "Hybrid beamforming for terahertz wireless communications: Challenges, architectures, and open problems," *IEEE Wireless Communications*, vol. 28, no. 4, pp. 198–204, 2021.

[13] A. Faisal, H. Sarieddeen, H. Dahrouj, T. Y. Al-Naffouri, and M.-S. Alouini, "Ultramassive mimo systems at terahertz bands: Prospects and challenges," *IEEE Vehicular Technology Magazine*, vol. 15, no. 4, pp. 33–42, 2020.

[14] H. Do, S. Cho, J. Park, H.-J. Song, N. Lee, and A. Lozano, "Terahertz line-of-sight mimo communication: Theory and practical challenges," *IEEE Communications Magazine*, vol. 59, no. 3, pp. 104–109, 2021.

[15] N. Maletic, L. Lopacinski, M. Goodarzi, M. Eissa, J. Gutierrez, and E. Grass, "A study of los mimo for short-range sub-thz wireless links," in *Mobile Communication-Technologies and Applications; 25th ITG-Symposium*. VDE, 2021, pp. 1–6.

[16] J. Wang, C.-X. Wang, J. Huang, H. Wang, X. Gao, X. You, and Y. Hao, "A novel 3d non-stationary gbsm for 6g thz ultra-massive mimo wireless systems," *IEEE Transactions on Vehicular Technology*, vol. 70, no. 12, pp. 12 312–12 324, 2021.

[17] Y. Chen, L. Yan, and C. Han, "Hybrid spherical-and planar-wave modeling and dcnn-powered estimation of terahertz ultra-massive mimo channels," *IEEE Transactions on Communications*, vol. 69, no. 10, pp. 7063–7076, 2021.

[18] Y. Chen, L. Yan, C. Han, and M. Tao, "Millidegree-level direction-of-arrival estimation and tracking for terahertz ultra-massive mimo systems," *IEEE Transactions on Wireless Communications*, vol. 21, no. 2, pp. 869–883, 2021.

[19] Z. Chen, X. Ma, C. Han, and Q. Wen, "Towards intelligent reflecting surface empowered 6g terahertz communications: A survey," *China Communications*, vol. 18, no. 5, pp. 93–119, 2021.

[20] Z. Chen, W. Chen, X. Ma, Z. Li, Y. Chi, and C. Han, "Taylor expansion aided gradient descent schemes for irs-enabled terahertz mimo systems," in *2020 IEEE Wireless Communications and Networking Conference Workshops (WCNCW)*. IEEE, 2020, pp. 1–7.

[21] A. Singh, M. Andrello, N. Thawdar, and J. M. Jornet, "Design and operation of a graphene-based plasmonic nano-antenna array for communication in the terahertz band," *IEEE Journal on Selected Areas in Communications*, vol. 38, no. 9, pp. 2104–2117, 2020.

[22] Z. Xu, X. Dong, and J. Bornemann, "Design of a reconfigurable mimo system for thz communications based on graphene antennas," *IEEE Transactions on Terahertz science and technology*, vol. 4, no. 5, pp. 609–617, 2014.

[23] S. A. Busari, K. M. S. Huq, S. Mumtaz, J. Rodriguez, Y. Fang, D. C. Sicker, S. Al-Rubaye, and A. Tsourdos, "Generalized hybrid beamforming for vehicular connectivity using thz massive mimo," *IEEE Transactions on Vehicular Technology*, vol. 68, no. 9, pp. 8372–8383, 2019.

[24] H. Sarieddeen, M.-S. Alouini, and T. Y. Al-Naffouri, "Terahertz-band ultra-massive spatial modulation mimo," *IEEE Journal on Selected Areas in Communications*, vol. 37, no. 9, pp. 2040–2052, 2019.

[25] A. A. Farid, A. S. Ahmed, A. Dhananjay, P. Skrimponis, S. Rangan, and M. Rodwell, "135ghz cmos/ltcc mimo receiver array tile modules," in *2021 IEEE BiCMOS and Compound Semiconductor Integrated Circuits and Technology Symposium (BCICTS)*. IEEE, 2021, pp. 1–4.

[26] S. Abu-Surra, W. Choi, S. Choi, E. Seok, D. Kim, N. Sharma, S. Advani, V. Loseu, K. Bae, I. Na *et al.*, "End-to-end 140 ghz wireless link demonstration with fully-digital beamformed system," in *2021 IEEE International Conference on Communications Workshops (ICC Workshops)*. IEEE, 2021, pp. 1–6.

[27] S. Park, A. Alkhateeb, and R. W. Heath, "Dynamic subarrays for hybrid precoding in wideband mmwave mimo systems," *IEEE Transactions on Wireless communications*, vol. 16, no. 5, pp. 2907–2920, 2017.

[28] K.-M. Luk, S.-F. Zhou, Y. Li, F. Wu, K.-B. Ng, C.-H. Chan, and S. Pang, "A microfabricated low-profile wideband antenna array for terahertz communications," *Scientific reports*, vol. 7, no. 1, p. 1268, 2017.

[29] G. D. Ntouni, T. Merkle, E. K. Loghis, G. Tzeranis, V. Koratzinos, N. D. Skentos, and D. Kritharidis, "Real-time experimental wireless testbed with digital beamforming at 300 ghz," in *2020 European Conference on Networks and Communications (EuCNC)*. IEEE, 2020, pp. 271–275.

[30] M. Elkhouly, M. J. Holyoak, D. Hendry, M. Zierdt, A. Singh, M. Sayginer, S. Shahramian, and Y. Baeyens, "D-band phased-array tx and rx front ends utilizing radio-on-glass technology," in *2020 IEEE Radio Frequency Integrated Circuits Symposium (RFIC)*. IEEE, 2020, pp. 91–94.

[31] V. Petrov, D. Bodet, and A. Singh, "Mobile near-field terahertz communications for 6g and 7g networks: Research challenges," *Frontiers in Communications and Networks*, vol. 4, p. 1151324, 2023.

[32] J. M. Jornet and I. F. Akyildiz, "Channel modeling and capacity analysis for electromagnetic wireless nanonetworks in the terahertz band," *IEEE Transactions on Wireless Communications*, vol. 10, no. 10, pp. 3211–3221, 2011.

[33] A. Goldsmith, *Wireless communications*. Cambridge university press, 2005.

[34] C. A. Balanis, *Antenna theory: analysis and design*. John wiley & sons, 2016.

[35] O. Tervo, I. Nousiainen, I. P. Nasarre, E. Tiirola, and J. Hulkkonen, "On the potential of using sub-thz frequencies for beyond 5g," in *2022 Joint European Conference on Networks and Communications & 6G Summit (EuCNC/6G Summit)*. IEEE, 2022, pp. 37–42.

[36] S. M. Alamouti, "A simple transmit diversity technique for wireless communications," *IEEE Journal on selected areas in communications*, vol. 16, no. 8, pp. 1451–1458, 1998.

[37] P. Sen, J. Hall, M. Polese, V. Petrov, D. Bodet, F. Restuccia, T. Melodia, and J. M. Jornet, "Terahertz communications can work in rain and snow: Impact of adverse weather conditions on channels at 140 ghz," in *Proceedings of the 6th ACM Workshop on Millimeter-Wave and Terahertz Networks and Sensing Systems*, 2022, pp. 13–18.

[38] D. Bodet, J. Hall, P. Sen, R. Johnson, I. Brandicourt, X. C. Roman, O. Shoura, and J. M. Jornet, "Data signals for terahertz communications research," *Computer Networks*, vol. 203, p. 108628, 2022.

[39] P. Sen, J. V. Siles, N. Thawdar, and J. M. Jornet, "Multi-kilometre and multi-gigabit-per-second sub-terahertz communications for wireless backhaul applications," *Nature Electronics*, vol. 6, no. 2, pp. 164–175, 2023.

[40] P. Sen, D. A. Pados, S. N. Batalama, E. Einarsson, J. P. Bird, and J. M. Jornet, "The teranova platform: An integrated testbed for ultra-broadband wireless communications at true terahertz frequencies," *Computer Networks*, vol. 179, p. 107370, 2020.

[41] M. Biguesh and A. B. Gershman, "Mimo channel estimation: optimal training and tradeoffs between estimation techniques," in *2004 IEEE International Conference on Communications (IEEE Cat. No. 04CH37577)*, vol. 5. IEEE, 2004, pp. 2658–2662.

[42] M. S. Rabbani, J. Churm, and A. Feresidis, "Electro-mechanically tunable meta-surfaces for beam-steered antennas from mm-wave to thz," in *2020 50th European Microwave Conference (EuMC)*. IEEE, 2021, pp. 416–419.

[43] H. Guerboukha, R. Shrestha, J. Neronha, O. Ryan, M. Hornbuckle, Z. Fang, and D. Mittleman, "Efficient leaky-wave antennas at terahertz frequencies generating highly directional beams," *Applied Physics Letters*, vol. 117, no. 26, 2020.

[44] D. Wang, J. Wang, X. You, Y. Wang, M. Chen, and X. Hou, "Spectral efficiency of distributed mimo systems," *IEEE Journal on Selected Areas in Communications*, vol. 31, no. 10, pp. 2112–2127, 2013.

[45] Y. Chen and C. Han, "Deep cnn-based spherical-wave channel estimation for terahertz ultra-massive mimo systems," in *GLOBECOM 2020-2020 IEEE Global Communications Conference*. IEEE, 2020, pp. 1–6.

[46] X. Ma, Z. Chen, W. Chen, Z. Li, Y. Chi, C. Han, and S. Li, "Joint channel estimation and data rate maximization for intelligent reflecting surface assisted terahertz mimo communication systems," *IEEE Access*, vol. 8, pp. 99 565–99 581, 2020.